Supporting Information

Synthesis, Biological Evaluation and Molecular Modeling of Donepezil and *N*-[(5-(Benzyloxy)-1-methyl-1*H*-indol-2-yl)methyl]-*N*-methylprop-2-yn-1-amine Hybrids, as New Multipotent Cholinesterase/Monoamine oxidase Inhibitors for the Treatment of Alzheimer's Disease

Irene Bolea,[±,#] Jordi Juárez-Jiménez,[&,#] Cristóbal de los Ríos,[‡] Mourad Chioua,[¶] Ramón Pouplana,[&] F. Javier Luque,[&] Mercedes Unzeta,[±,*] and José Marco-Contelles[¶,*] Abdelouahid Samadi[¶,]

Departament de Bioquímica i Biología Molecular, Facultat de Medicina. Institut de Neurociències. Universitat Autònoma de Barcelona, 08193 Bellaterra, Barcelona, Spain; Departament de Fisicoquímica, Facultat de Farmàcia, and Institut de Biomedicina (IBUB), Universitat de Barcelona, Av. Diagonal 643, E-08028, Barcelona, Spain; Laboratorio de Radicales Libres y Química Computacional (IOG, CSIC), Juan de la Cierva 3, E-28006, Madrid, Spain; Instituto Teófilo Hernando, Fundación de Investigación Biómedica, Hospital Universitario de la Princesa, C/ Diego de León, 62, E-28029, Madrid, Spain

[#] *Those authors have contributed equally to this work.*

Table of contents

Figure S1. Time (ns) evolution of the potential energy (x 10^3; kcal/mol) for the MD simulations of (*top; left*) the AChE-donepezil complex, and the complexes of **5** bound to (*top; right*) AChE(1EVE), (*bottom; left*) AChE(2CKM) and (*bottom; right*) AChE(1Q83).

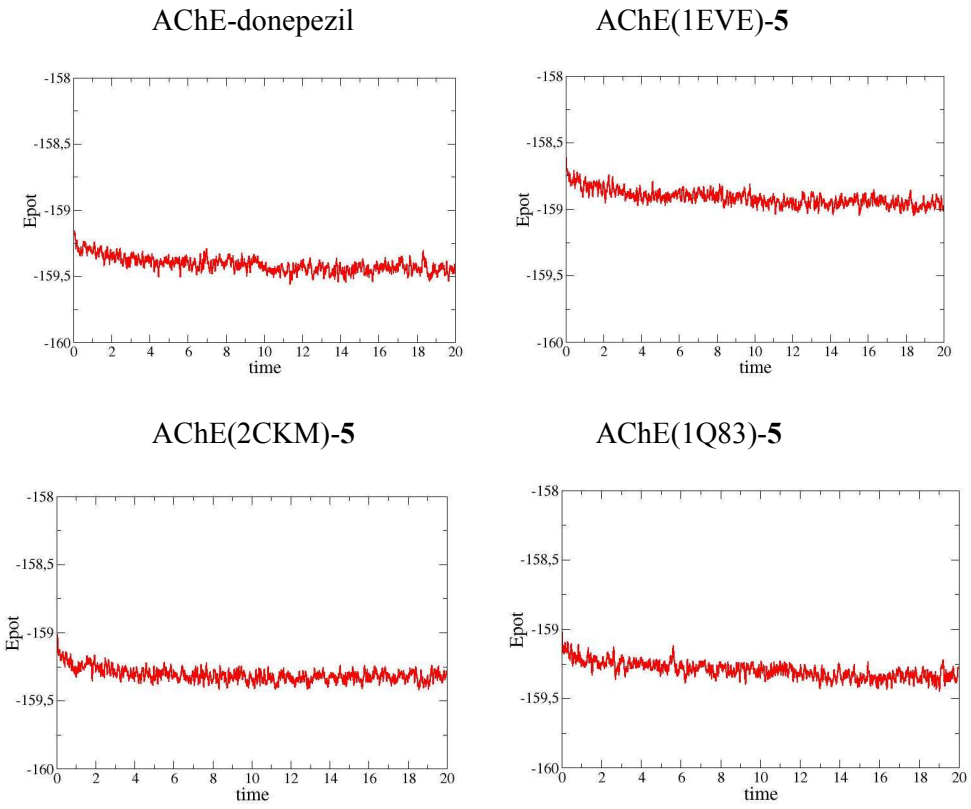

Figure S2. Time (ns) evolution of the positional root-mean square deviation (RMSD; Å) for the MD simulations of (*top; left*) the AChE-donepezil complex, and the complexes of **5** bound to (*top; right*) AChE(1EVE), (*bottom; left*) AChE(2CKM) and (*bottom; right*) AChE(1Q83). The RMSD was determined for the backbone atoms (black), and the heavy atoms of the residues that delineate the binding site (red) relative to the energy minimized structure of each AChE-**5** complex.

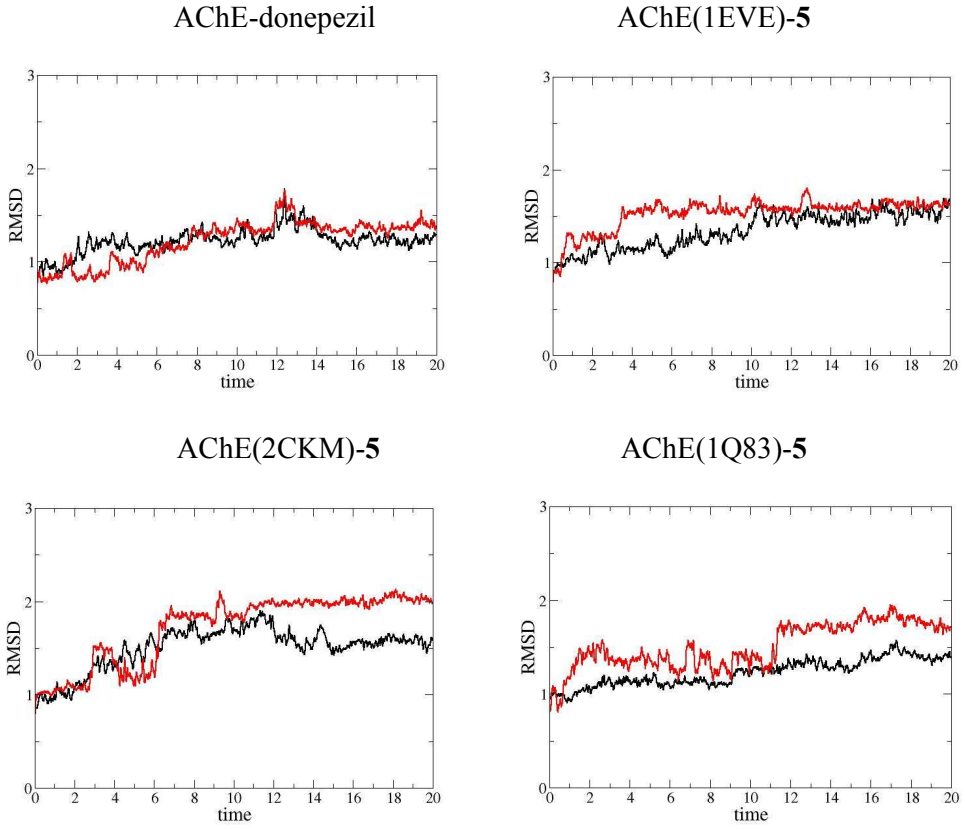

Figure S3. Time (ns) evolution of the torsional angles (degrees) that define the orientation of the side chain of Trp279 for the MD simulations of (*top; left*) AChE-donepezil complex, and the complexes of **5** bound to (*top; right*) AChE(1EVE), (*bottom; left*) AChE(2CKM) and (*bottom; right*) AChE(1Q83). Dihedral angles N–C_α–C_β–C_γ and C_α–C_β–C_γ–C_δ are shown in orange and blue, respectively.

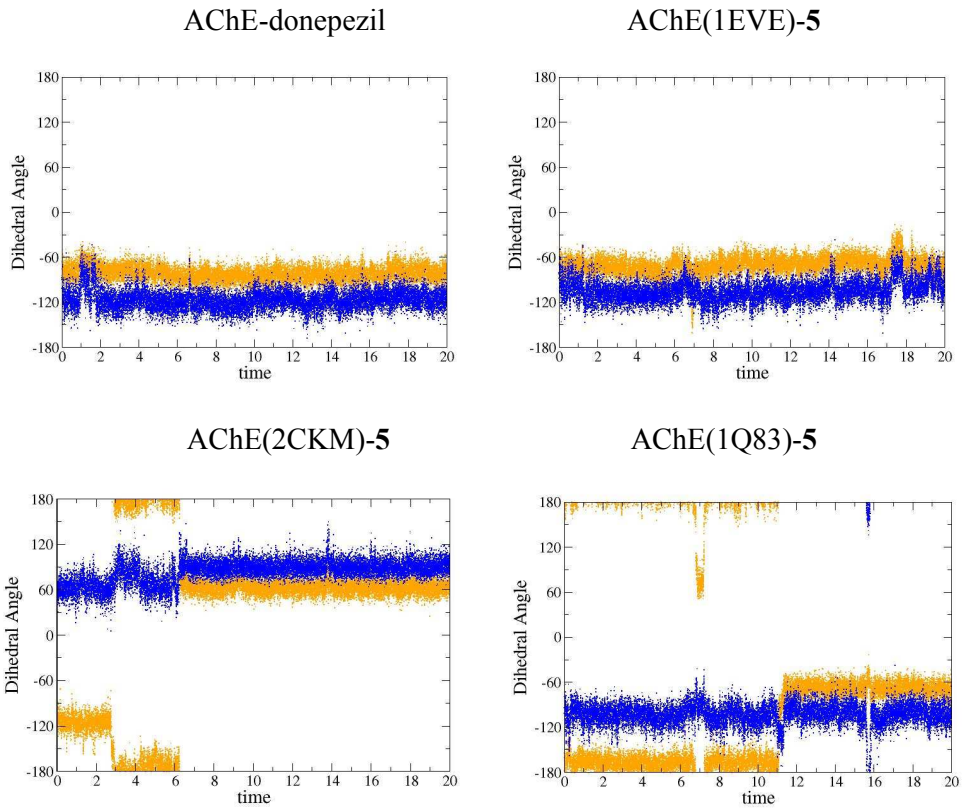

Figure S4. Representation of the binding mode of (*top*) donepezil and (*bottom*) **5** bound to AChE. The binding mode of donepezil is taken from the X-ray structure (PDB entry 1EVE). For the binding of **5** to AChE(1EVE), five snapshots taken every ns along the last 5 ns of the trajectory are superposed. Selected residues in the binding site are shown as yellow (X-ray) and green (AChE(1EVE)) sticks, whereas the ligand is shown as orange (donepezil) and blue (**5**) sticks.

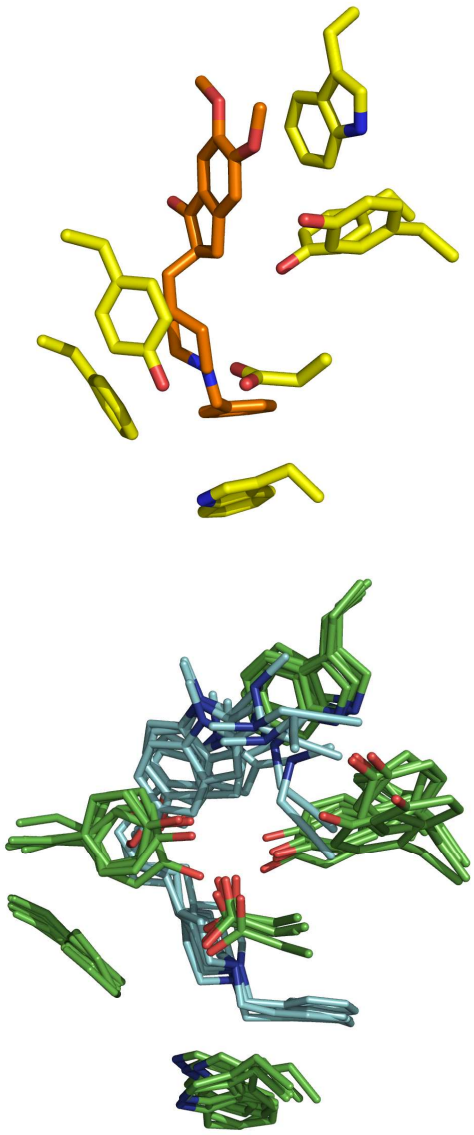

Figure S5. View of the stacking interaction formed by the indole ring of **5** with the aromatic rings of Tyr334 and Trp279. Shortening or lengthening of the tether should be accompanied by displacements of the indole ring along the gorge that would increase the stacking against Tyr334 or Trp279.

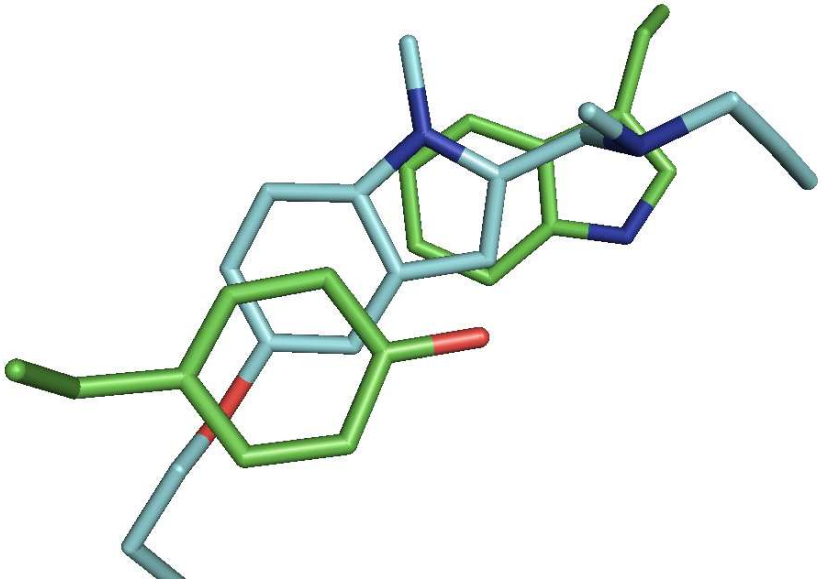

Figure S6. View of the spatial location of residues Asp70 and Glu198 in the CAS for (*top*) the X-ray structure of the complex between AChE (yellow) and donepezil (orange), and (*bottom*) the complex between AChE(1EVE) (green) and **5** (blue). Selected distances are given in angstroms.

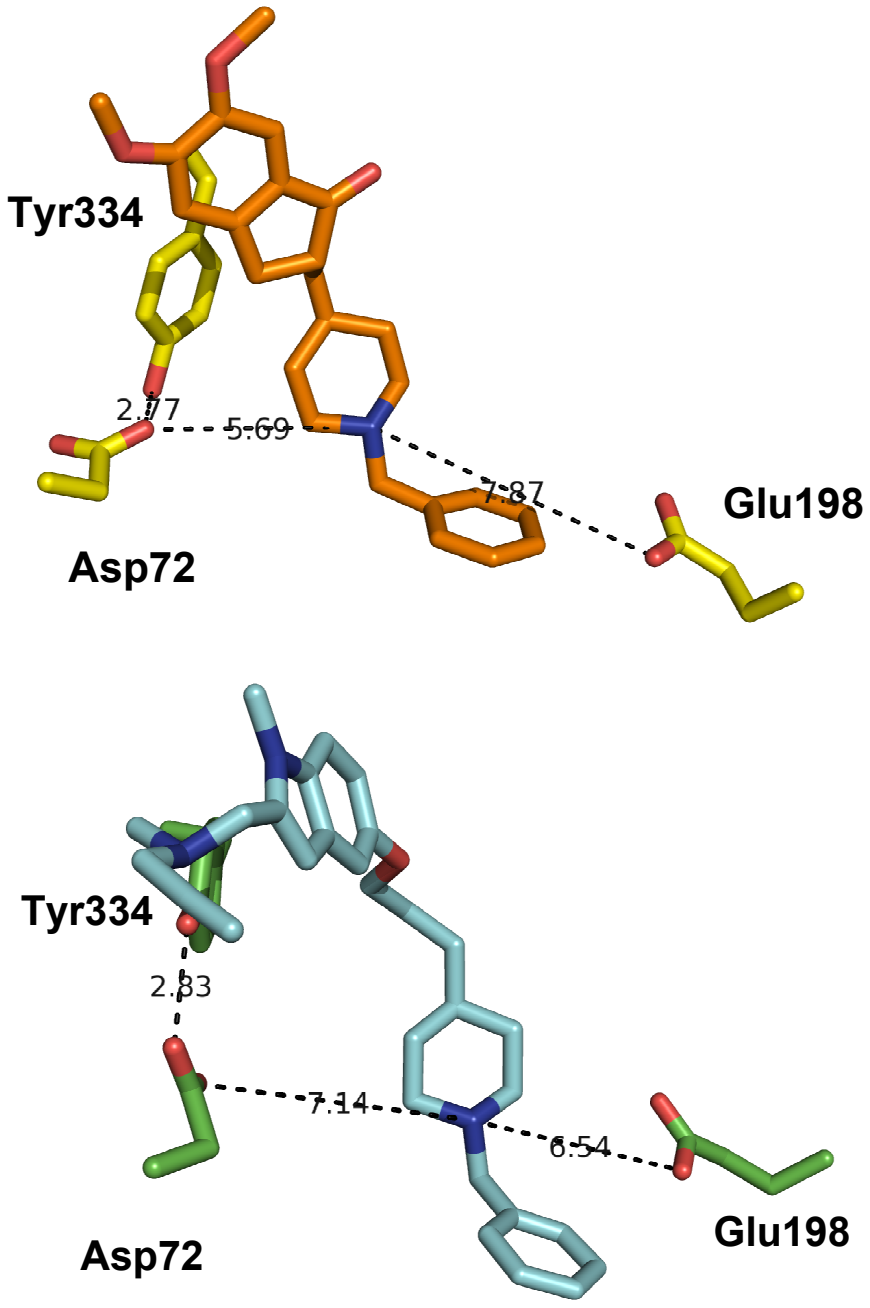

Figure S7. Representation of the inverted binding mode of **5** in the binding site of AChE for the AChE_1EVE model. Superposition of the snapshots taken every 2 ns along the last 10 ns of the trajectory for the complex with (top) AChE_1EVE, (middle) AChE_1Q83 and (bottom) AChE_2CKM. The ligand is shown in orange, and selected residues at the CAS (Trp84, Phe330) and PAS (Tyr70, Trp279) are shown in green.

ACHE_1EVE

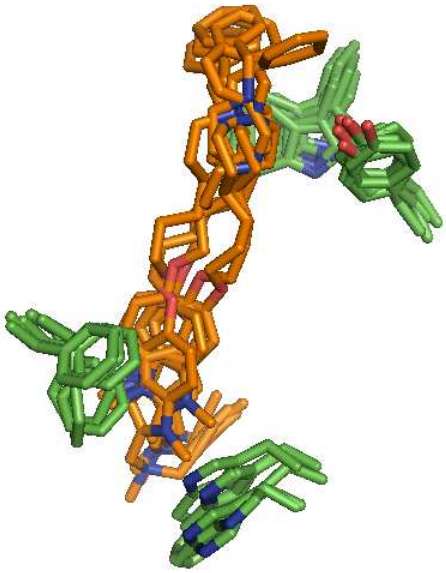

ACHE_1Q83

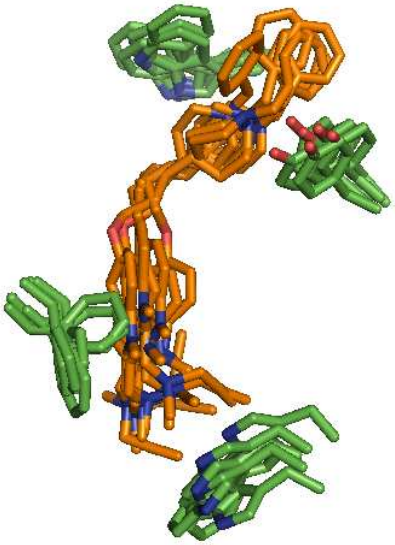

ACHE_2CKM

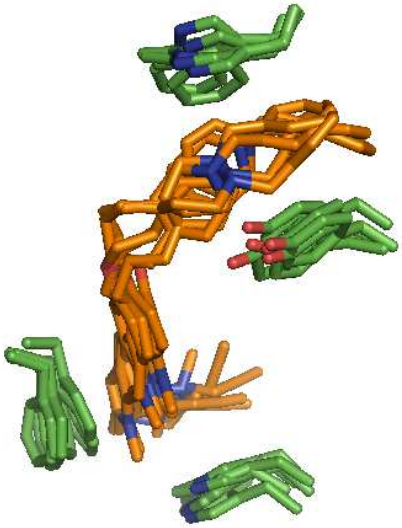

Figure S8. Representation of poses 1, 3, 5, 7 and 12 (covering a range of 5 kcal/mol in the score) obtained upon docking of compound **5** (blue) into the binding site of BuChE. Selected residues in the binding site of BuChE are also shown (green) together with the residue numbered in the enzyme (PDB entry 2PM8), and the corresponding residues in AChE.

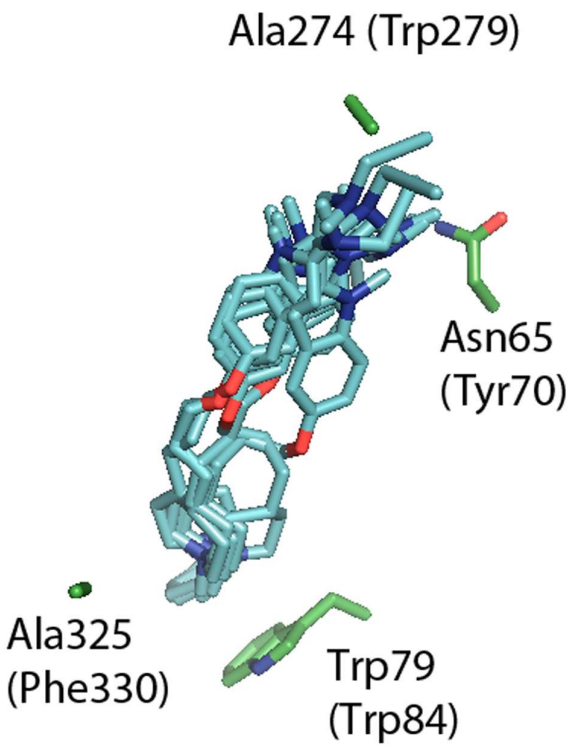

Figure S9. Time (ns) evolution of the potential energy (x 10^3; kcal/mol) for the MD simulations of **5** noncovalently bound to (*top*) MAO-A and (*bottom*) MAO-B.

MAO-A

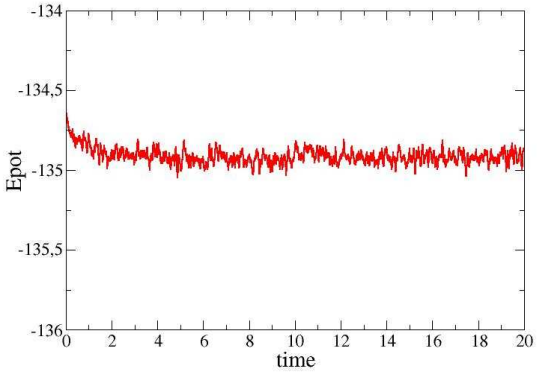

MAO-B

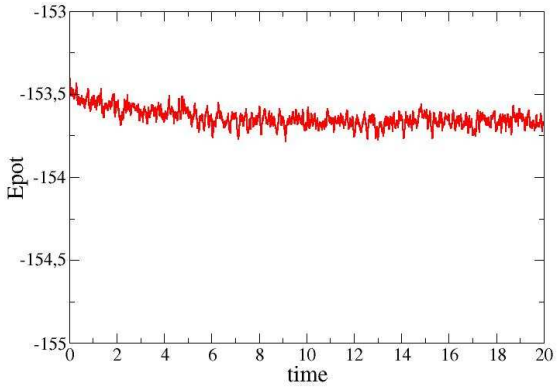

Figure S10. Time (ns) evolution of the positional root-mean square deviation (RMSD; Å) for the MD simulations of hybrid **5** bound to (*top*) MAO-A and (*bottom*) MAO-B. The RMSD was determined for the backbone atoms (black) and the heavy atoms of the residues that delineate the binding site (red).

MAO-A

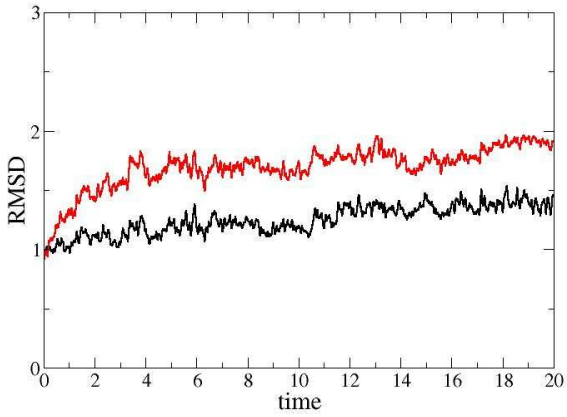

MAO-B

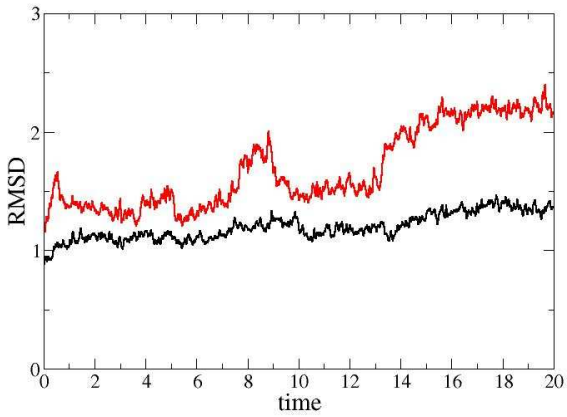

Figure S11. (*Top*) Superposition of the last snapshot obtained from the MD simulation run for the MAO-A complex of **5** with harmine (shown as magenta sticks) as found in the X-ray structure of its complex to human MAO-A (PDB entry 2Z5X). (*Bottom*) Superposition of the initial (yellow sticks) and final snapshots of the 20 ns MD simulation run for the MAO-A-**5** complex.

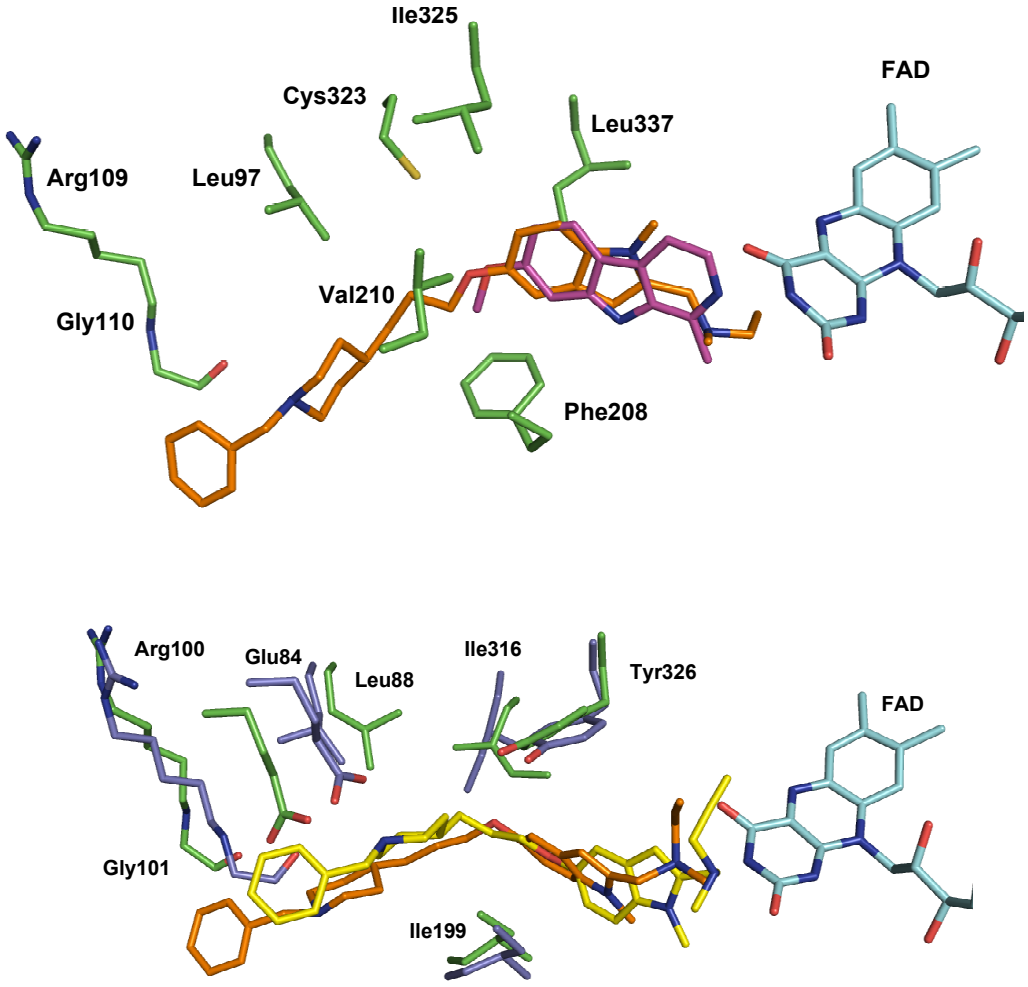

Figure S12. (*Top*) Superposition of the last snapshot obtained from the MD simulation run for the MAO-B complex of **5** with deprenyl (shown as magenta sticks) and rasagiline (shown as white sticks) as found in the X-ray structures of their complexes to human MAO-B (PDB entries 2BYB and 1S2Q, respectively). (*Bottom*) Superposition of the initial (yellow sticks) and final snapshots of the 20 ns-MD simulation run for the MAO-A-**5** complex.

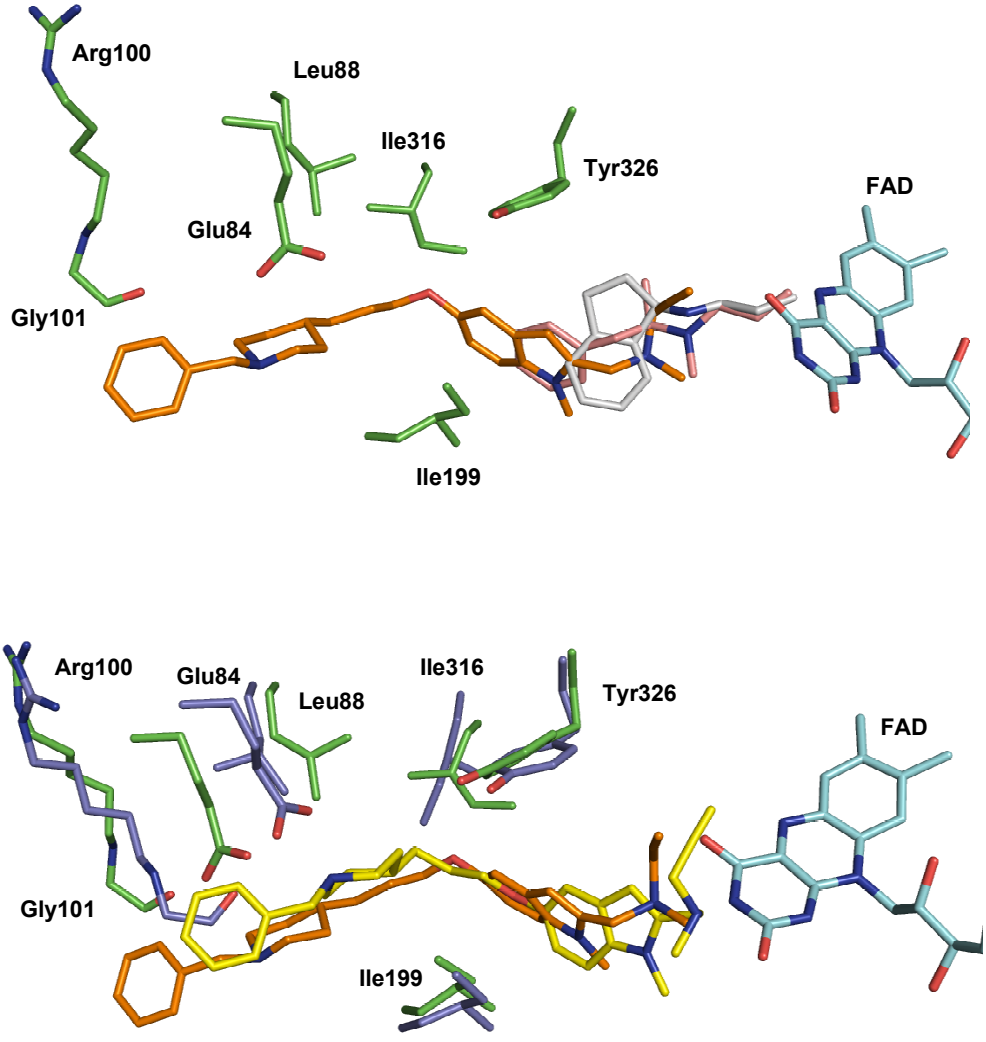

Figure S13. Time evolution (ns) of the distance (Å) from the carbon atom that bears the protonated amine in **5** to the nitrogen atom involved in chemical modification of FAD by deprenyl and rasagiline. Profiles for MAO-A and MAO-B are shown in blue and orange, respectively.

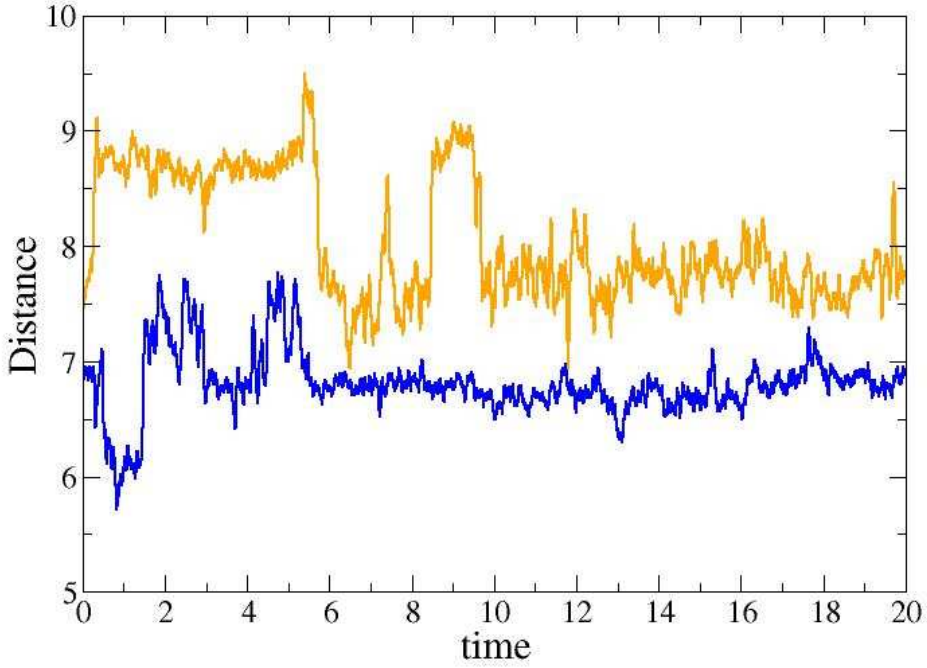

Figure S14. Time (ns) evolution of the potential energy (x 10^3; kcal/mol) for the MD simulations of **5** covalently bound to (*top*) MAO-A and (*bottom*) MAO-B.

MAO-A

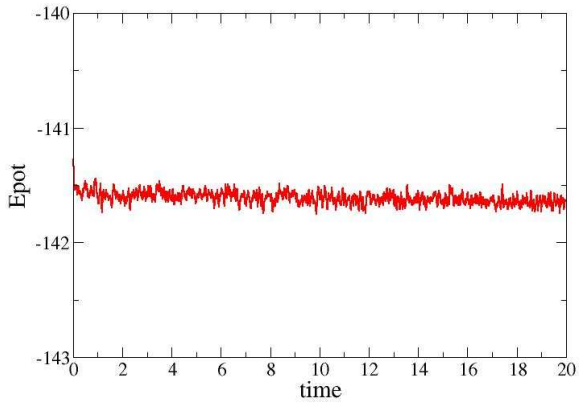

MAO-B

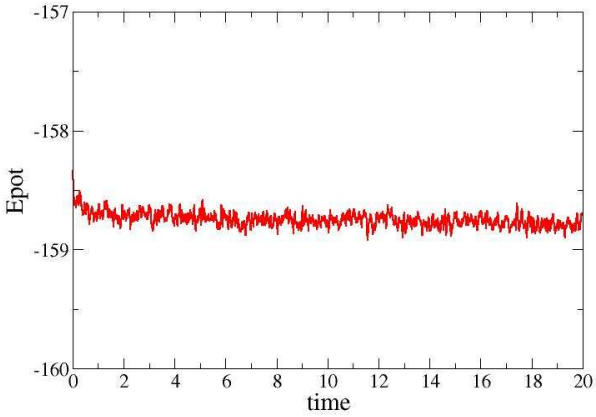

Table S1. MM–PBSA analysis of the binding affinity (kcal/mol) of compound **5** to AChE(1EVE) and AChE(2CKM). Calculations were performed for a set of 100 snapshots taken during the last 5 ns of the simulations (A) using standard atomic radii implemented in AMBER force field, and (B) the atomic radii optimized for MM/PBSA calculations with the AMBER force field.

A) Standard atomic radii.

Target	ΔG_{MM} (ele/vW)	ΔG_{ele}^{sol}	$\Delta G_{non-polar}^{sol}$	$\Delta G_{binding}$	$\Delta\Delta G_{binding}$
1EVE	-500.4 (-443.5/-56.9)	470.9	-7.3	-36.8	0.0
2CKM	-511.9 (-455.2/-53.2)	484.6	-7.3	-34.5	+2.3

B) Optimized atomic radii

Target	ΔG_{MM} (ele/vW)	ΔG_{ele}^{sol}	$\Delta G_{non-polar}^{sol}$	$\Delta G_{binding}$	$\Delta\Delta G_{binding}$
1EVE	-500.4 (-443.5/-56.9)	444.9	-7.3	-62.7	0.0
2CKM	-511.9 (-455.2/-53.2)	460.6	-7.3	-58.7	+4.0

Table S2. MM–PBSA analysis of the relative stability (kcal/mol) of the different complexes between **5** and AChE(1EVE) and AChE(2CKM). Normal and inverted denote the orientation with the benzylpiperidine moiety in the CAS or in the PAS, respectively. Calculations were performed for a set of 100 snapshots taken during the last 5 ns of the simulations using standard atomic radii implemented in AMBER force field.

Target	$\Delta\Delta G_{MM}$	$\Delta\Delta G_{ele}^{sol}$	$\Delta\Delta G_{non-polar}^{sol}$	$\Delta\Delta G_{binding}$
Normal orientation				
1EVE	0.0	0.0	0.0	0.0
2CKM	-29.3	149.2	-1.6	118.2
Inverted orientation				
1EVE	-69.6	175.2	-3.3	102.3
1Q83	-2.0	69.4	-1.4	65.9
2CKM	-9.0	124.1	-2.4	112.6

Since the initial state of the binding process of **5** to AChE is common for all the different complexes, the relative stability of the distinct binding modes can be directly taken from the comparison of the stabilities of the bound state (i.e., the AChE-**5** complex), which takes into account not only the interaction between ligand and protein, but also the contribution due to structural deformations.

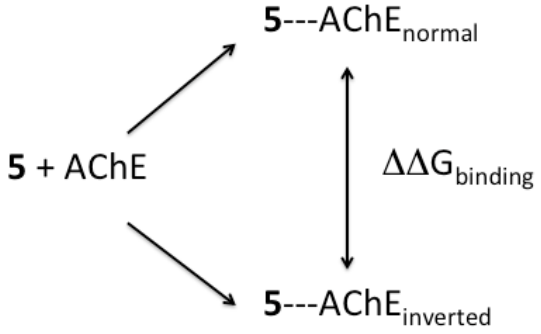

Table S3. MM–PBSA analysis of the binding affinity (kcal/mol) of compound **5** to MAO-A and MAO-B. Calculations were performed for a set of 100 snapshots taken during the last 5 ns of the simulations using standard atomic radii implemented in AMBER force field.

a) Simulation of compound **5** in the binding site prior to chemical reaction with FAD. Data determined for the whole ligand.

Target	ΔG_{MM} (ele/vW)	ΔG_{ele}^{sol}	$\Delta G_{non-polar}^{sol}$	$\Delta G_{binding}$
MAOA	-127.1 (-66.5/-60.6)	108.4	-7.1	-25.7
MAOB	-253.1 (-194.3/-58.8)	219.6	-7.1	-40.5

b) Simulation of compound **5** in the binding site prior to chemical reaction with FAD. Data determined for a truncated ligand where the propargyl unit has been replaced by a dummy atom.

Target	ΔG_{MM} (ele/vW)	ΔG_{ele}^{sol}	$\Delta G_{non-polar}^{sol}$	$\Delta G_{binding}$
MAOA	-104.6 (-51.9/-52.7)	89.0	-7.0	-22.6
MAOB	-225.5 (-172.6/-52.4)	193.2	-7.0	-38.8

c) Simulation of the adduct formed by compound **5** after chemical reaction with FAD. Data determined for a truncated ligand where the propargyl unit has been replaced by a dummy atom.

Note that due to the covalent linkage with FAD, there is a substantial charge redistribution in the ligand, which affects the magnitude of ΔG_{MM} and ΔG_{ele}^{sol} in MM/PBSA calculations compared to the noncovalently form of **5**. Therefore, caution is required for the comparison of the separate free energy components in the noncovalent and covalent forms of the inhibitor.

Target	ΔG_{MM} (ele/vW)	ΔG_{ele}^{sol}	$\Delta G_{non-polar}^{sol}$	$\Delta G_{binding}$
MAOA	-69.7 (-14.4/-55.3)	50.7	-7.0	-26.0
MAOB2	-167.0 (-105.3/-61.7)	129.6	-7.0	-44.4